18 March 1983, Volume 219, Number 4590 **SCIENCE**

Electrophoresis: Mathematical Modeling and Computer Simulation

M. Bier, O. A. Palusinski, R. A. Mosher, D. A. Saville

The extraordinary usefulness of electrophoretic techniques for the analysis of protein mixtures was first demonstrated by Tiselius (*1*) with his elegant moving boundary apparatus, which resolved human serum proteins into albumin and the four globulin fractions, α_1, α_2, β, and γ. This original discovery gave rise to a steady development of new instruments and techniques with ever-increasing resolution. Currently, two-dimensional electrophoresis, combined with sophisticated computer-image analysis, can resolve several thousand proteins among the products of a given cell type (*2*). The most important of the innumerable applications of electrophoresis are in molecular biology and medicine.

Summary. A mathematical model of electrophoretic separation processes has been developed and adapted for computer simulations. The model is used to predict the characteristic behavior of a variety of electrophoretic techniques from a knowledge of chemical equilibria and physical transport phenomena. The model provides a unifying basis for a rational classification of all electrophoretic processes.

Most materials in aqueous solution acquire an electrical charge due to ionization and therefore move in response to an external electric field. The charged entities may be simple ions, complex macromolecules, colloids, or living cells (*3–8*). The rate of migration depends on the amount of charge, the size and shape of the particle, and the properties of the solvent. Resolution is increased by the imposition of other constraints, such as molecular sieving or *p*H gradients. In addition, certain migrating species may be positively identified through the use of specific antibodies. A systematic, logical classification of the rather bewildering choice of analytical and preparative techniques is difficult, but four classical modes of electrophoresis are generally recognized (*3–8*): moving boundary electrophoresis (MBE), zone electrophoresis (ZE), isotachophoresis (ITP), and isoelectric focusing (IEF). Each may be employed in a variety of techniques. For instance, IEF was first developed with density gradients for fluid stabilization (*9*), but is now mainly used in polyacrylamide or agarose gels (*10, 11*) and has also been adapted to continuous flow (*12*) as well as to a recycling mode of operation (*13*). Although existing theories may explain the principal features of a particular mode or technique, they are usually predicated on conditions too restrictive to permit generalization. Thus, models that describe Tiselius' MBE cannot be used to predict the course of events in ZE, and models of ITP do not explain IEF. Yet there are many reasons to believe that all electrophoretic processes can be understood by use of a few axiomatic principles and that a single, general quantitative theory can be synthesized. In this article, we describe such a model and demonstrate its applicability for computer simulation of electrophoretic processes (*14*). The model also provides the basis for a scientific classification and comparison of electrophoretic techniques. In addition, simulation facilitates the development of new separation methods.

Although it is not our intention to review all of the electrophoretic methodologies or the theories that describe them, it is helpful to mention some of the distinguishing features of the four classical modes. In MBE, the analysis is based on the migration rate of moving boundaries formed by components of differing mobilities. The fastest component forms the leading boundary in the ascending arm of the Tiselius cell, the slowest component the trailing boundary in the descending arm. Complete separation of components is never achieved (*15*). In ZE, the sample occupies a much smaller portion of the column and complete separation of sample constituents is possible. Whereas both MBE and ZE are usually carried out in homogeneous buffers, discontinuous electrolyte systems must be used in ITP (*6, 16*), the sample being inserted between the leading and terminating electrolytes. At steady state, all constituents migrate at the same speed, in the order of their net mobilities. The formation of these boundaries has been studied extensively (*17*). Isoelectric focusing differs from the other classical modes in that it depends on the formation of a stable *p*H gradient wherein the sample constituents migrate to their isoelectric points (*18, 19*).

For a qualitative appreciation of the principal features common to all electrophoretic processes, an understanding of Kohlrausch's 1897 study (*20*) is essential. Kohlrausch established a general principle which can be restated as follows: the passage of an electric current through an electrolyte system causes changes only where the system is nonhomogeneous. Thus, the imposition of an electric current on a homogeneous solution leaves the local concentrations intact. Three types of inhomogeneities were considered. The most obvious occurs at the interface of the electrode and

---

M. Bier is a professor and R. A. Mosher is a research associate at the Biophysics Technology Laboratory and O. A. Palusinski is associate professor of electrical engineering at the University of Arizona, Tucson 85721. D. A. Saville is a professor of chemical engineering at Princeton University, Princeton, New Jersey 08544.

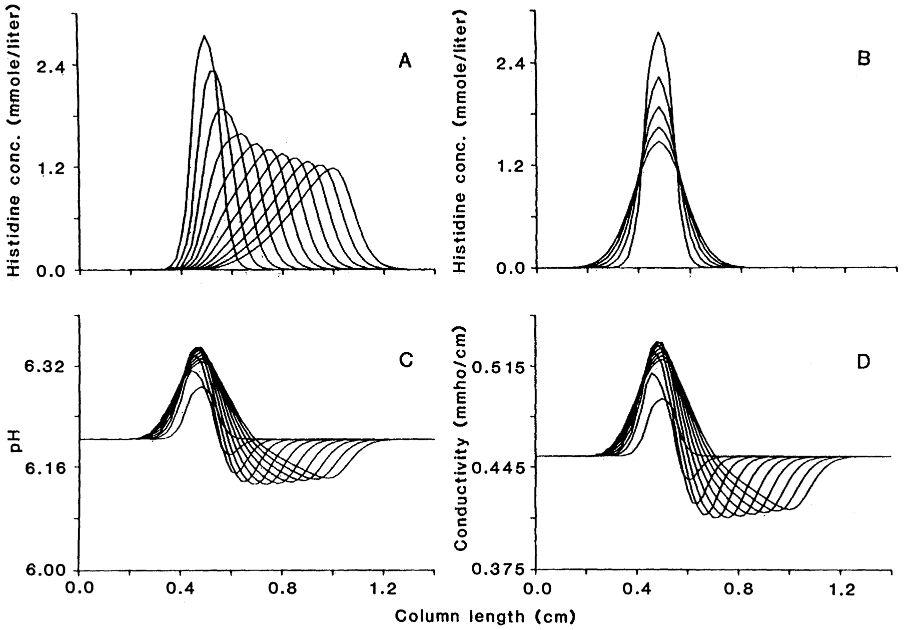

Fig. 1. Simulation of zone electrophoresis. Initial conditions: uniform distribution of 20 m*M* cacodylate and 10 m*M* tris throughout the column. The histidine zone is 3 m*M*. (A) Zone electrophoresis of histidine, at 1.2-minute intervals for a total of 12 minutes. (B) Diffusion only of histidine at 3-minute intervals, for a total of 12 minutes. The *p*H (C) and conductivity profiles (D) for (A).

the solution where electrochemical reactions produce concentration changes and give rise to new species, as first described by Hittorf in 1853 (*21*). These effects are avoided in MBE, ZE, and ITP by using large electrode buffer volumes. In IEF, however, reactions at the electrodes may be utilized to generate the *p*H gradient (*19*). A second type of inhomogeneity occurs at the boundary between two different ionic species. Here the electric current causes the migration of the boundary. The advancing boundary may either degrade with time as a result of diffusion, or be self-stabilizing as predicted by Kohlrausch. The latter condition requires specific mobility relationships between constituent ions and forms the basis of ITP (*6, 16*). The third type of inhomogeneity is a concentration gradient caused by simple dilution of an electrolytic solution. Such a gradient is largely unaffected by the electric current, but broadens as a result of diffusion. The "stationary boundaries" in the Tiselius apparatus are an example.

Our model represents the four electrophoretic modes and their inherent species and concentration gradients by a set of partial differential equations coupled to nonlinear algebraic relations. The modes differ only in their initial conditions—that is, the distribution of components along the axis of the electrophoretic column—and the boundary conditions that describe the ion permeabilities at the ends of the column. The implications of these two conditions will become evident from our simulation studies. The mathematical model was used to develop a computer program designed to predict the time-dependent evolution of electrophoretic systems involving biprotic ampholytes. It extends our earlier work on modeling the steady and transient states in IEF (*19*).

Reaction Equilibria, Transport Rates, and Conservation Relations

The key parameters governing the behavior of an electrophoretic system are the dissociation constants and electrophoretic mobilities of the components. Ionic dissociation-association rates are rapid relative to transport by diffusion and electromigration. The ionization equilibria for water and each biprotic ampholyte are represented by the well-known equations

$$K_w = [H^+]\,[OH^-] \tag{1}$$

$$K_{j1} = \frac{[H^+][A_j^0]}{[A_j^+]} \tag{2}$$

$$K_{j2} = \frac{[H^+][A_j^-]}{[A_j^0]} \tag{3}$$

These equations involve three species per ampholyte (A_j^0, A_j^+, and A_j^-) in addi-

Table 1. Initial conditions used in computer simulations. Left and right boundaries refer to the orientation of the computer plots. The assignment of anode and cathode depended on the net charge of histidine, that is, the *p*H. The mobilities (μ, expressed in units of 10^{-4} cm^2/V-sec) and pK values used in the simulations were: cacodylate, $\mu = 2.31$ and $pK = 6.21$; tris, $\mu = 2.41$ and $pK = 8.30$; and histidine, $\mu = 2.02$ and $pK_1 = 6.04$, $pK_2 = 9.17$.

Electrophoretic mode	Boundary	Polarity	Cacodylate (m*M*)	Tris (m*M*)	Histidine (m*M*)	Conductivity (mmho/cm)	*p*H	Current (mA/cm^2)
Zone electrophoresis	Left	Anode	20.0	10.0	0*	0.452	6.20	3.16
	Right	Cathode	20.0	10.0	0*	0.452	6.20	
Moving boundary	Left	Anode	19.4	10.5	0.0	0.475	6.27	3.69
descending arm	Right	Cathode	20.0	10.0	3.0	0.496	6.29	
Moving boundary	Left	Anode	20.0	10.0	3.0	0.496	6.29	3.69
ascending arm	Right	Cathode	19.4	10.5	0.0	0.475	6.27	
Isotachophoresis	Left	Cathode	0.0	50.0	40.0	0.514	8.80	1.50
lower concentration	Right	Anode	20.0	50.0	0.0	0.907	8.48	
Isotachophoresis	Left	Cathode	0.0	50.0	40.0	0.514	8.80	1.04
higher concentration	Right	Anode	60.0	50.0	0.0	2.200	6.83	
Isoelectric focusing	Left	Anode	8.76	8.27	7.05	0.365	7.22	0.08
	Right	Cathode	8.76	8.27	7.05	0.365	7.22	
Electrodialysis	Left	Cathode	23.9	45.3	0†	1.08	8.26	1.57
	Right	Anode	23.9	45.3	0†	1.08	8.26	

*A histidine zone with a peak concentration of 3 m*M* was located in the center of the column. †A histidine membrane with a peak concentration of 100 m*M* was assigned to the center of the column.

tion to H^+ and OH^-. Water is assumed to be in excess and thus the total number of species is $3L + 2$, where L is the number of ampholytes. The other dependent variable is the field strength, $-\nabla\phi$, where ϕ is the electric potential measured in volts. It follows that we need $3L + 3$ relations to calculate the local changes in concentration and potential.

Each species migrates by diffusion and, if charged, by electromigration. The flux is related to the field strength and concentration gradient by

$$F_i = -M_i z_i \Omega_i \nabla\phi - \frac{RT}{e} \Omega_i \nabla M_i \quad (4)$$

where F_i is the flux in moles per square meter per second, z_i is the valence, Ω_i the mobility coefficient (square meters per volt per second), R the gas constant (8.314 kg-m^2/sec^2-K), T the absolute temperature (Kelvin), and e the molar charge or Faraday constant (96,500 coulombs per mole). The symbols used to represent the concentrations (expressed in moles per cubic meter) are: $[H^+] = M_1$, $[OH^-] = M_2$, $[A_j^0] = M_{3j}$, $[A_j^+] = M_{3j+1}$, $[A_j^-] = M_{3j+2}$, where $j = 1, 2, \ldots, L$. The mobility coefficient is related to the diffusivity by the Einstein expression $D_i = RT\Omega_i/e$. Furthermore, in the absence of bulk flow, each species is governed by a conservation law

$$\frac{\partial}{\partial t} M_i = -\nabla \cdot F_i + R_i \quad (5)$$

where R_i is the rate of generation of the ith species (moles per cubic meter per second). Since the rate of production of each ampholyte is nil

$$R_{3j} + R_{3j+1} + R_{3j+2} = 0 \quad (6)$$

Upon combining this with the conservation law we obtain

$$\frac{\partial}{\partial t} (M_{3j} + M_{3j+1} + M_{3j+2})$$

$$= -\nabla \cdot (F_{3j} + F_{3j+1} + F_{3j+2}) \quad (7)$$

This expression provides L equations, one for each ampholyte.

Next we require the rate of charge generation to be zero except at the electrodes.

$$\sum_{1}^{3L+2} e z_i R_i = 0 \quad (8)$$

It can also be shown that electroneutrality prevails on the scale of interest. Hence

$$\sum_{1}^{3L+2} e z_i M_i = 0 \quad (9)$$

Combining the last two equations with the conservation relation (Eq. 5), we obtain the charge conservation relation in terms of the current as

$$\nabla \cdot \sum_{1}^{3L+2} e z_i F_i = 0 \quad (10)$$

This gives $L + 2$ equations; L equations representing ampholyte conservation, one equation expressing electrical neutrality, and one equation for the current. The remaining $2L + 1$ equations come from the ionic equilibria for water (Eq. 1) and for each ampholyte (Eqs. 2 and 3).

Thus far, our efforts have been focused on one-dimensional, isothermal systems, but even here the set of equations is nonlinear, and numerical methods are required to construct solutions. The potential gradient as well as all the species concentrations are computed during the integration, so that we can avoid ad hoc stipulations regarding the pH profile or the voltage gradient. Simple acids and bases can easily be accommodated by suppressing the appropriate dissociation constants. Electroosmosis or any other bulk flow is not considered.

The presence of algebraic relations (Eqs. 1 to 3) as well as of partial differential equations (Eq. 7) complicates the numerical solution of the problem. The model must be put in dimensionless form to provide the proper physical scaling, and in some situations, the expressions fall into the class of stiff differential equations. The procedure we have been using consists of discretizing the spatial derivatives at a set of grid points to generate a set of ordinary differential equations, with time as the independent variable. The resulting equations are integrated numerically with DARE-P simulation software (*22*). Calculations were carried out with a CDC-Cyber-175 processor.

Simulation of Electrophoretic Processes

Although our treatment is amenable to more complex systems, we decided to use the simplest system sufficient to illustrate the essential characteristics of the four electrophoretic modes. The components included a weak acid, a weak base, and an ampholyte—specifically, cacodylic acid, tris(hydroxymethyl)aminomethane (tris), and histidine.

In each simulation, the appropriate initial and boundary conditions must be specified. The initial conditions are summarized in Table 1 and are partially illustrated in the graphics. Although a constant current was assumed in all cases, the model can be adapted to simulate processes with constant voltage or power. The initial concentrations and current were chosen for illustrative purposes and varied from one case to another. Equally

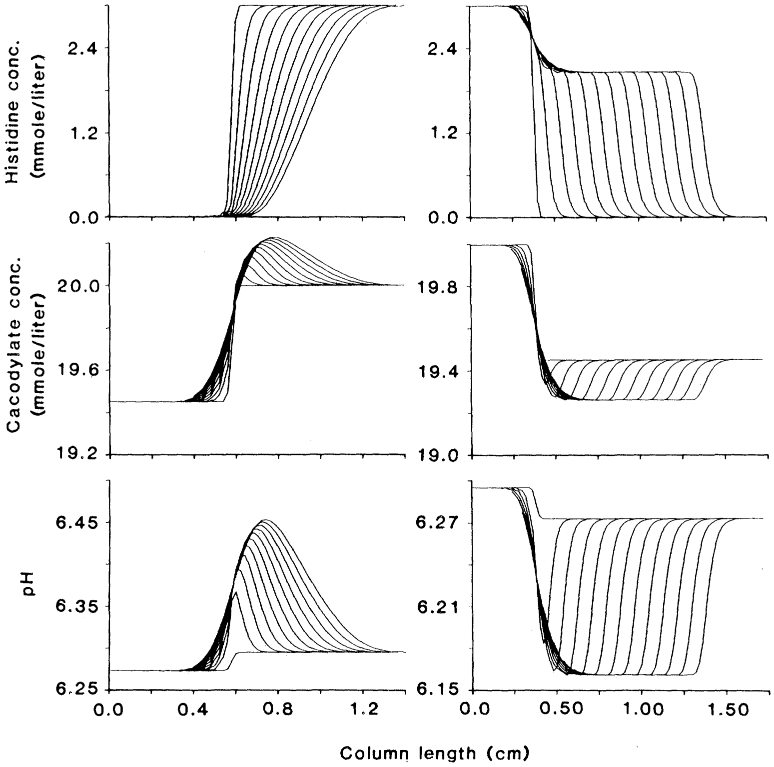

Fig. 2. Simulation of moving boundary electrophoresis. Initial concentrations were similar to those of Fig. 1. (Left) Descending arm of the simulated Tiselius cell at 1.2-minute intervals for a total of 12 minutes. (Right) Ascending arm at 1.8-minute intervals for a total of 21.6 minutes.

arbitrary was the choice of the electrolytes assigned the functions of "sample" and "buffers." For instance, although histidine was used as the migrating "sample" in ZE and MBE, either the acid or the base could have been so used. It should also be stated that histidine is far more interactive with the "buffer" electrolytes cacodylic acid and tris than a protein sample would be, since the net mobility and dissociation of most proteins are less sensitive to *p*H. A simulation of electrodialysis (ED)—that is, electrophoretic ion transport across a charged membrane—was included to demonstrate the versatility of the model.

The boundary conditions for IEF differed from those for the other modes; for IEF, the ends of the column were assumed to be permeable only to hydrogen and hydroxyl ions, whereas in all other instances, unrestricted permeability was specified. This reflects the usual experimental arrangements; the large electrode buffer volumes customarily used in MBE, ZE, and ITP assure constancy of buffer composition at the ends of the electrophoretic columns, whereas in IEF often only minimal volumes of strong acid and base are used at the electrodes. For IEF and ED, a stationary grid was used, but for the other modes a movable grid was adopted to define an "observational window." Our algorithm advances this window at the migration rate of the leading species.

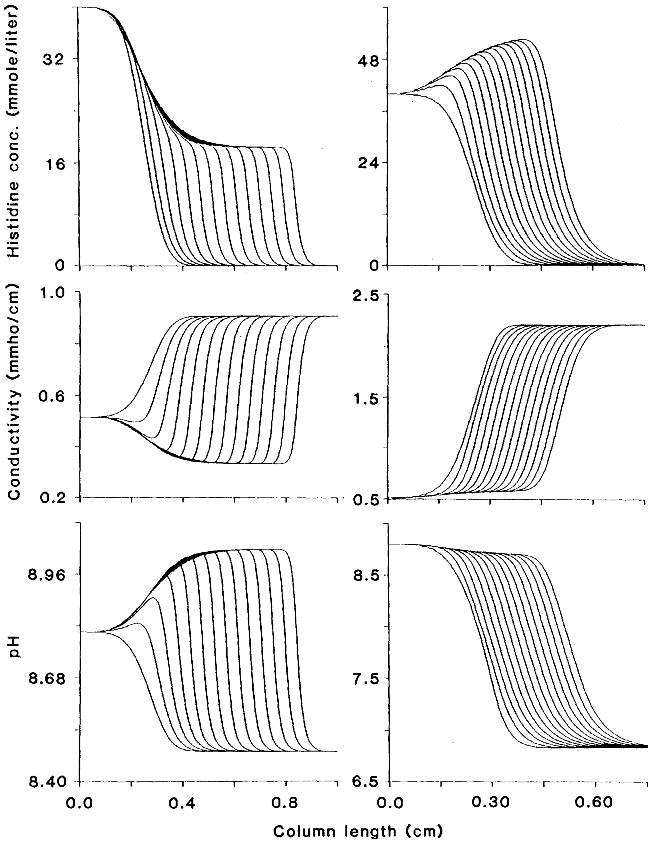

Fig. 3. Simulation of isotachophoresis. Leader: cacodylate, 20 m*M* (left plots) and 60 m*M* (right plots). Terminator: 40 m*M* histidine. Counterion: 50 m*M* tris. (Left) Downward Kohlrausch concentration adjustment, 2-minute intervals for a total of 26 minutes. (Right) Upward adjustment at 4-minute intervals for a total of 52 minutes.

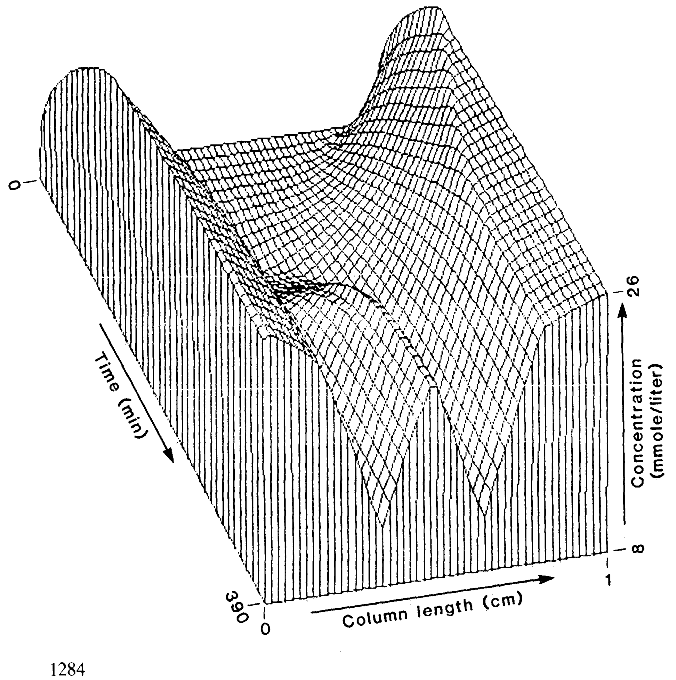

Fig. 4. Computer-generated three-dimensional plot of the concentration profiles in isoelectric focusing. Initial condition: uniform distribution of 7.16 m*M* cacodylate, 8.27 m*M* tris, and 7.05 m*M* histidine. Only the predominant component along the column axis is shown, cacodylate at the left, histidine in the middle, and tris at the right. Focusing time, 390 minutes.

Zone Electrophoresis

The pertinent data used in this simulation are listed in Table 1. The buffer consisted of 20 m*M* cacodylate and 10 m*M* tris, *p*H 6.20, and was initially distributed uniformly throughout the column, whereas the 3 m*M* histidine sample was placed at the center of the observational window in a Gaussian concentration distribution. In this buffer mixture, histidine has a positive net charge and migrates toward the cathode. Figure 1A shows the evolution of the histidine concentration profiles at 1.2-minute intervals for a total of 12 minutes. Their symmetry is lost, the leading edge becoming sharper than the trailing one. This is to be compared with Fig. 1B, where an identical system in the absence of current shows diffusion only of histidine; the distribution remains Gaussian as the zone spreads without losing its symmetry. The peak concentration of the histidine after 12 minutes of diffusion is substantially higher than that after 12 minutes of ZE, since "trailing" is avoided. The addition of the histidine sample to the buffer background causes an initial local increase in *p*H and conductivity (Fig. 1, C and D). During ZE, these perturbations become more pronounced, evolving into complex curves. The *p*H and conductivity profiles remain symmetrical in the case of pure diffusion and are not displayed. The cause of the patterns' complexity will become obvious from the simulation of MBE.

Moving Boundary Electrophoresis

In ZE, the histidine sample was assumed to have been superimposed on a uniform concentration of the cacodylate-tris buffer. For MBE, similar concentrations were used, except that the histidine was assumed to have been equilibrated by dialysis against the buffer. Thus, the composition of the buffer changes across the sample boundary as a result of the Donnan equilibrium (*23*) (see Table 1).

The descending and ascending arms of the simulated Tiselius cell were computed separately and are presented on the left and right sides of Fig. 2. In each case, the buffer-equilibrated sample occupied half of our observational window, the buffer the other half. The evolution of the histidine boundaries shown in the top panels differs radically between the two arms. The descending arm shows the expected migration of the boundary and its broadening due to diffusion. In the ascending arm, there is an initial readjustment of histidine concentration; its profile remains unchanged thereafter. This behavior is typical of ITP and results from the formation of a mixed histidine-cacodylate isotachophoretic step. The average mobility of the cacodylate-histidine mixture is lower than the net mobility of cacodylate ion alone, which is a necessary condition for ITP. The common counterion is tris. Separation of histidine from cacodylate is impossible because of the imposed infinite supply of both ions at the ends of the observational window. The center row in Fig. 2 shows the corresponding profiles of the advancing cacodylate boundary at the sample-buffer interface. The initial step discontinuity in cacodylate concentration is due to Donnan's equilibrium. The descending boundaries are again characterized by diffusional spreading, whereas the ascending boundaries are self-adjusting. Similar behavior is exhibited by the *p*H profiles shown in the bottom row of Fig. 2. There is a significant drop in *p*H across the sample-buffer boundary in the ascending arm and a *p*H increase across the descending arm. Conductivity profiles were similar and are therefore not reproduced.

The similarity to ZE (Fig. 1) is obvious. The ascending arm in MBE mimics the frontal boundary in ZE, the descending arm reflecting the trailing boundary in ZE. Superimposition of the two profiles yields the sinuous curves obtained for conductivity and *p*H in ZE. Thus, the formation of the mixed isotachophoretic step explains the loss of symmetry in the ZE histidine plots.

Isotachophoresis

For the initial distribution of components, cacodylic acid was assumed to be the leading ion, histidine the terminator, and tris the common counterion. At the chosen concentrations, histidine was negatively charged and had a lower net mobility than cacodylate (see Table 1). In Fig. 3, histidine occupies the cathodic (left) side of the column and cacodylate the anodic end. The three-component system is sufficient to form a single isotachophoretic boundary. The system differs from the ascending branch of MBE, where the terminator was a mixed zone of histidine and cacodylate.

Two simulations were performed to show the model's ability to reproduce the self-adjusting decrease (left side of Fig. 3) or increase (right side of Fig. 3) of histidine concentration predicted by Kohlrausch (*20*). This required different input concentrations of the leading ion, cacodylate, but the other concentrations were unchanged. The graphs are largely self-explanatory and clearly demonstrate the model's ability to generate the expected adjustments in concentration, which are in exact agreement with the Kohlrausch regulating function.

Isoelectric Focusing

The boundary conditions differ in IEF since it is assumed that the current across the ends of the column is carried only by hydrogen and hydroxyl (*21*) and that all changes originate at the electrodes, propagating toward the center. This is reflected in the much-delayed central focusing of histidine, as com-

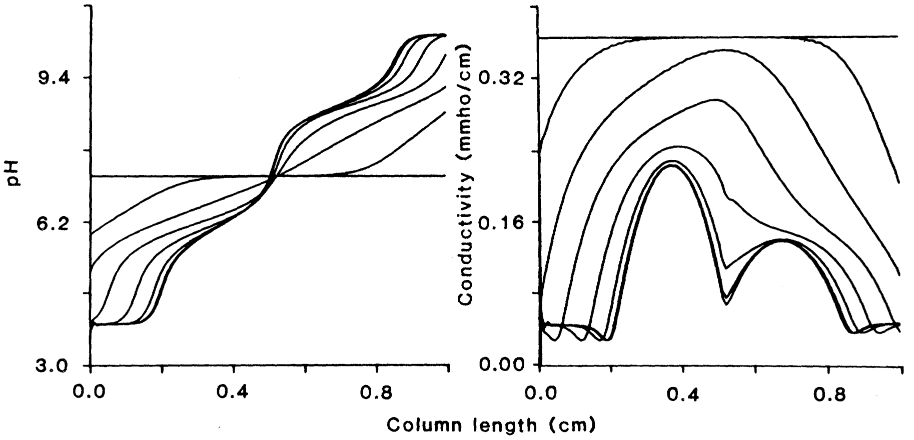

Fig. 5. *p*H and conductivity profiles for Fig. 4. Times are 0, 30, 90, 150, 210, 270, 330, and 390 minutes of isoelectric focusing.

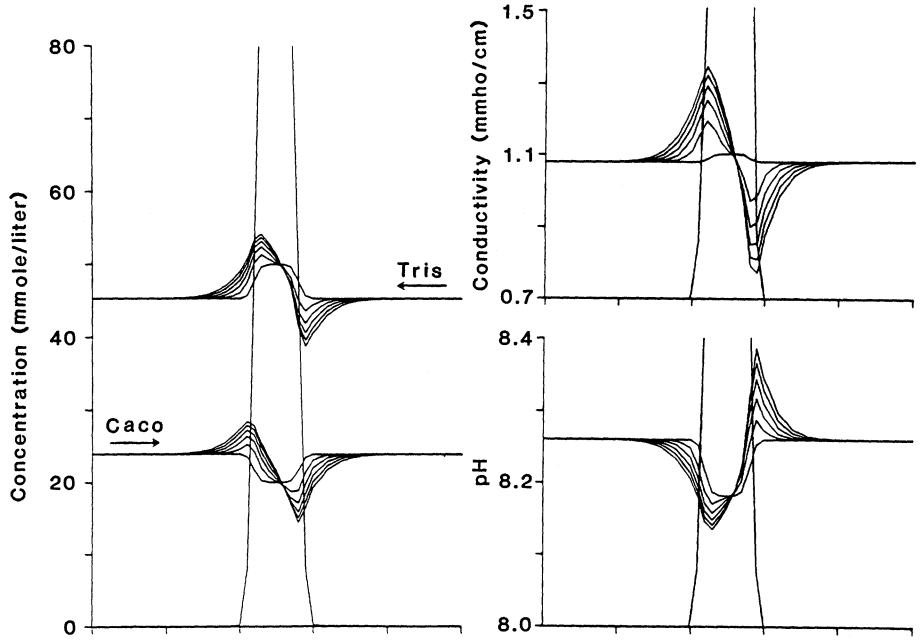

Fig. 6. Simulation of electrodialysis. The nearly vertical lines represent a 100 m*M* histidine membrane in Gaussian distribution. The buffer was 23.9 m*M* cacodylate and 45.3 m*M* tris, *p*H 8.26. (Left) Polarization of cacodylate (*Caco*) at the cathodic side of the membrane with depletion of tris at the anodic side. (Right) Conductivity and *p*H plots. Plots at 2-minute intervals for a total of 10 minutes.

pared to the focusing of acid and base (Fig. 4). The final profiles resulting from the transient model were identical to those obtained by our earlier steady-state model (*19*).

The evolution of the *p*H and conductivity profiles is shown in Fig. 5. An initial uniform distribution of all three components was assumed, represented by the horizontal lines in all plots. Profiles are shown after 30 minutes of focusing and at hourly intervals thereafter, for a total of 390 minutes of focusing at constant current density. The conductivity profiles clearly show the generation of "conductivity gaps," regions of lower conductivity at the ends of the column and near its center. These coincide with accumulation of undissociated acid, base, and ampholyte, as shown in our earlier computations of the steady state in IEF (*19*).

Electrodialysis

Electrodialysis is widely used for desalting aqueous solutions (*24*) and relies on ion-permselective membranes; membranes formed from anion-exchange resins allow the preferential electrical transport of anions and tend to reject cations, while those incorporating cation-exchange resins display reversed selectivity.

In our simulation, a stationary solution containing cacodylic acid and tris, *p*H 8.26, was assumed to be electrodialyzed across a membrane incorporating 100 m*M* histidine, immobilized in Gaussian distribution. The negatively charged histidine membrane was initially equilibrated by dialysis against the electrolyte mixture. Donnan's equilibrium resulted in an initial increase in tris concentration within the membrane and a decrease in cacodylate concentration. When a current was imposed, the negatively charged membrane rejected the cacodylate ions, causing them to accumulate at the cathodic side. As a result, most of the current across the membrane is carried by tris ions, causing their depletion from the anodic side. These concentration polarizations and the corresponding *p*H and conductivity profiles are shown in Fig. 6.

Discussion and Future Directions

Our objective was to demonstrate that diverse electrophoretic processes can be described by a single mathematical model and computation scheme. The model was constructed from fundamental equations describing mass transport, dissociation equilibria, conservation of mass and charge, and the principle of electroneutrality, thereby avoiding most of the restrictive assumptions inherent in earlier models and simulations (*15–17*).

The computation scheme is capable not only of simulating features of ZE, MBE, ITP, and IEF, but also reveals details of boundary structures (concentration, *p*H, conductivity), not easily amenable to direct experimental observation. It is important to note that the four modes differ only in the initial distribution of components along the electrophoretic column and the boundary permeability—stipulations that can be traced to Kohlrausch (*20*) and Hittorf (*21*). The Kohlrausch-Hittorf constraints can be seen as defining an "electrophoretic plane," wherein these four modes represent idealized points within a virtually infinite gradation of possibilities.

The many actual electrophoretic techniques in current use require constraints not considered by Kohlrausch and Hittorf. Examples of these constraints are specific affinities, as in immunoelectrophoresis; molecular sieving, as in high density polyacrylamide gels; cross-flow, as in continuous flow electrophoresis; counterflow, as occasionally utilized in ITP; magnetic fields, as in electromagnetophoresis; fixed charges, as in IEF with immobilized *p*H gradients; charged membrane barriers, as in ED; and neutral membrane barriers, as in electrodecantation or forced-flow electrophoresis. Some of these constraints can be easily incorporated into the present program, as demonstrated for ED. Molecular sieving can be modeled by making the mobility of a species dependent on its position along the column axis. Systems involving bulk fluid motion, such as cross-flow electrophoresis (*25*), would require substantial model modification. Nevertheless, a logical classification of electrophoretic techniques emerges in terms of their location within a multidimensional "electrophoretic space," characterized by initial and boundary conditions as well as the other possible constraints.

Simulation can also facilitate the development of new separation techniques by exploration of constraints not yet realized in the laboratory, such as the imposition of selective ion permeabilities at the boundaries. The program is already being used for the formulation of optimized buffer mixtures for IEF in the absence of commercial carrier ampholytes. Although a five-component program is now available, further expansion is desirable. The inclusion of noninteractive protein "samples," that is, proteins present in trace quantities, is easily accomplished, but more complicated extensions are also envisaged. In addition, experimental validation studies are in progress. One impediment is the paucity of reliable data on mobilities and dissociation constants. Comparison between experimental results and computer simulation may help to refine these data.

Despite the simplifications that attend each of the aforementioned electrophoretic modes, it should be recognized that each contains elements of all the fundamental modes. The overall similarities between ZE and MBE, and the presence of an ITP step in the ascending arm of MBE, have been illustrated. Furthermore, *p*H gradients are intrinsic features of electrophoresis, and elements of IEF may be present in many separations. Indeed, it is clear that adjusting the initial distribution of components and controlling boundary permeabilities produce a wide variety of electrophoretic processes, some of which have heretofore eluded study.

References and Notes

1. A. Tiselius, *Trans. Faraday Soc.* **33**, 524 (1937).
2. P. H. O'Farrell, *J. Biol. Chem.* **250**, 4007 (1975): N. L. Anderson, *Trends Anal. Chem.* **1**, 131 (1982); D. W. Sammons, L. D. Adams, E. E. Nishizawa, *Electrophoresis* **2**, 135 (1981).
3. Reviews of electrophoretic processes abound, but most of the work relevant to this study may be found in (*4–8*).
4. M. Bier, Ed., *Electrophoresis: Theory, Methods, and Applications* (Academic Press, New York, 1959), vol. 1.
5. ———, *ibid.* (Academic Press, New York, 1967), vol. 2.
6. F. M. Everaerts, J. L. Beckers, T. P. E. M. Verheggen, *Isotachophoresis: Theory, Instrumentation, and Applications* (Elsevier, Amsterdam, 1976).
7. Z. Deyl, Ed., *Electrophoresis: A Survey of Techniques and Applications* (Elsevier, Amsterdam, 1979).
8. P. G. Righetti, C. J. van Oss, J. W. Vanderhoff, Eds., *Electrokinetic Separation Methods* (Elsevier/North-Holland, Amsterdam, 1979).
9. H. Svensson, *Arch. Biochem. Biophys. Suppl.* **1**, 132 (1962).
10. R. J. Radola and D. Graesslin, Eds., *Electrofocusing and Isotachophoresis* (de Gruyter, Berlin, 1977).
11. H. Haglund, J. G. Westerfeld, J. T. Ball, Eds., *Electrofocus/78* (Elsevier/North-Holland, New York, 1979).
12. J. S. Fawcett, *Ann. N.Y. Acad. Sci.* **209**, 112 (1973); P. Basset, C. Froissart, G. Vincendon, R. Massarelli, *Electrophoresis* **1**, 168 (1980).
13. M. Bier and N. B. Egen, in (*11*), pp. 35–48; ———, T. T. Allgyer, G. E. Twitty, R. A. Mosher, in *Peptides: Structure and Biological Function*, E. Gross and J. Meienhofer, Eds. (Pierce Chemical Co., Rockford, Ill., 1979), pp. 79–90.
14. We use the term "electrophoresis" in the generic sense to denote transport processes of charged species in dilute aqueous solutions resulting from an applied d-c electric field.
15. L. G. Longsworth, in (*4*), pp. 91–136 and 137–177; V. P. Dole, *J. Am. Chem. Soc.* **67**, 1119 (1945); J. Vacik in (*7*), pp. 1–22.
16. M. Bier and T. T. Allgyer, in (*8*), pp. 443–470; A. J. P. Martin and F. M. Everaerts, *Anal. Chim. Acta* **38**, 233 (1967); G. T. Moore, *J. Chromatogr.* **106**, 1 (1975).
17. E. Schumacher and T. Studer, *Helv. Chim. Acta* **47**, 957 (1964); E. Schumacher, W. Thormann, D. Arn, in *Analytical Isotachophoresis*, F. M. Everaerts, Ed. (Elsevier, Amsterdam, 1981), pp. 33–39; P. Ryser, thesis, University of Bern, Switzerland (1976); W. Thormann, thesis, University of Bern, Switzerland (1982): P. Radi, thesis, University of Bern, Switzerland (1982).
18. H. Svensson, *Acta Chem. Scand.* **15**, 325 (1961);

H. Rilbe (formerly H. Svensson) in *Isoelectric Focusing*, N. Catsimpoolas, Ed. (Academic Press, New York, 1976), pp. 13–52; M. Almgren, *Chem. Scr.* **1**, 69 (1971); G. H. Weiss, N. Catsimpoolas, D. Rodbard, *Arch. Biochem. Biophys.* **163**, 106 (1974); J. R. Cann and K. S. Gardiner, *Biophys. Chem.* **10**, 203 (1979).
19. O. A. Palusinski, T. T. Allgyer, R. A. Mosher, M. Bier, D. A. Saville, *Biophys. Chem.* **13**, 193 (1981); M. Bier, R. A. Mosher, O. A. Palusinski, *J. Chromatogr.* **211**, 313 (1981); O. A. Palusinski, M. Bier, D. A. Saville, *Biophys. Chem.* **14**, 389 (1981).
20. F. Kohlrausch, *Ann. Phys. (Leipzig)* **62**, 209 (1897).
21. J. W. Hittorf, *Poggendorff's Ann.* **89**, 177 (1853).
22. G. A. Korn and J. V. Wait, *Digital Continuous System Simulation* (Prentice-Hall, Englewood Cliffs, N.J., 1978).
23. F. G. Donnan, *Chem. Rev.* **1**, 73 (1924).
24. N. Lakshminarayanaiah, *Transport Phenomena in Membranes* (Academic Press, New York, 1969).
25. D. A. Saville, *Phys. Chem. Hydrodyn.* **1**, 297 (1980).
26. This work was supported in part by NASA contract NAS8-32950, NASA grant NSG-7333, and NSF grant CPE 8103079. We thank A. Graham and W. P. Maynard for their contributions to the development of the program. The programs for both steady state and transient state are available on request.

Fire Mosaics in Southern California and Northern Baja California

Richard A. Minnich

Summary. In spite of suppression efforts, severe wildfires burn large areas of southern California grassland, coastal sage scrub, and chaparral. Such large burns may not have been characteristic prior to the initiation of fire suppression more than 70 years ago. To compare controlled with uncontrolled areas, wildfires of southern California and adjacent northern Baja California were evaluated for the period 1972 to 1980 from Landsat imagery. Fire size and location, vegetation, year, and season were recorded. It was found that suppression has divergent effects on different plant communities depending on successional processes, growth rates, fuel accumulation, decomposition rates, and length of flammability cycles. These variables establish feedback between the course of active fires, fire history, spatial configuration of flammable vegetation, and fire size. Suppression has minimal impact in coastal sage scrub and grassland. Fire control in chaparral reduces the number of fires, not burned hectarage; fires consequently increase in size, spread rate, and intensity and become uncontrollable in severe weather conditions. The Baja California chaparral fire regime may serve as a model for prescribed burning in southern California.

Wild-land fire, which has been a feature of the southern California landscape throughout historic time and into the recent geologic past (*1*), is a symptom of the prevailing Mediterranean climate. Winter rains nourish extensive carpets of shrubs and grasses; the long summer drought parches them. Dead twigs, foliage, and litter accumulate in vast quantities because of limited microbial decomposition (*2, 3*). Inevitably, fires kindle and spread, fuel and weather permitting.

Spanish and Anglo-European shepherds and farmers living in the Los Angeles coastal plain before the 20th century expressed little concern over mountain fires, even when they reported (*4, 5*) fires burning for months until extinguished by autumn rains. However, with rapid agricultural expansion and urbanization beginning around 1880, the preservation of natural vegetation was recognized as central to the prevention of watershed erosion and flooding (*6*). In 1892 the mountain public domain was federalized as the nation's first forest reserve. Fire suppression was part of this change in jurisdiction.

In recent years, land managers have become increasingly interested in the concept of setting small, controllable fires to prevent excessive fuel accumulation and catastrophic blazes (*7, 8*). This attempt to change the fire pattern requires understanding the impact of fire suppression on vegetation. Since fire suppression has been a long-standing policy, there is no wild landscape in southern California in which such suppression has not been practiced, thus precluding comparisons. Investigators of the fire ecology of California brush and grasslands (*9*) have attempted to reconstruct past fire frequency and stand mosaics from fire scars and dendrochronology (*10*), newspapers, government expeditions, diaries, and old photographs (*5*). The fragmentary nature of such data has been severely limiting to the reconstruction efforts.

Although a similar landscape without fire control exists in neighboring northern Baja California, a formal compilation of Baja California fires was impossible until the 1972 launch of the orbiting Landsat platform. Using this new source of information, I reconstructed the fire history of southern California and adjacent Baja California for the period 1972 to 1980, and thus determined the consequences of fire suppression in grassland, coastal sage scrub, and chaparral. I found that a fire suppression strategy that attempts to extinguish all fires before they become large may promote large burns in some vegetation types. A few fires burning in severe weather easily escape control and denude large areas.

The Physical Environment

The area analyzed extends from 35°N in southern California to 30°N in northern Baja California (Fig. 1). Terrain is mostly mountainous, with scattered coastal plains, alluvial valleys, and basins. Mountain ranges form two distinct structural units: the west-to-east oriented Transverse Ranges (western Transverse Ranges and the Santa Monica, San Gabriel, and San Bernardino Mountains) and the northwest-southeast trending Peninsular Ranges (the Santa Ana, San Jacinto, Palomar, and Laguna Mountains, Sierra Juárez, and Sierra San Pedro Mártir).

Winter precipitation, which results largely from frontal disturbances of the polar front jet stream, decreases southward along the coast from 400 millimeters per year at Los Angeles to 250 millimeters at San Diego and Ensenada

---

Richard A. Minnich is an assistant professor in the Geography Program, Department of Earth Sciences, University of California, Riverside 92521.